A01-31441

AIAA 2001-3071
Numerical Simulation of Gas Flow Over Micro-Scale Airfoils

Q. Sun and I.D. Boyd
University of Michigan
Ann Arbor, MI

G.V. Candler
University of Minnesota
Minneapolis, MN

35th AIAA Thermophysics Conference
11-14 June 2001 / Anaheim, CA

AIAA 2001-3071

NUMERICAL SIMULATION OF GAS FLOW OVER MICRO-SCALE AIRFOILS

Quanhua Sun* and Iain D. Boyd†
Department of Aerospace Engineering
University of Michigan, Ann Arbor, MI, 48109

Graham V. Candler‡
Department of Aerospace Engineering and Mechanics
University of Minnesota, Minneapolis, MN 55455

Abstract

Flows over micro-scale airfoils are investigated using both particle and continuum approaches. An implementation of the information preservation technique based on the direct simulation Monte Carlo method is used to simulate flows over a flat plate of zero thickness at low Reynolds number (Re<100), and good agreement is obtained comparing with experimental data and theoretical results. Investigation shows that the aerodynamics of a 5% flat plate at Re=4 is quite different from that at Re=4,000 that were measured experimentally. A continuum approach with slip boundary conditions predicts a similar basic flow pattern as the IP method with differences in details, which may indicate that continuum approaches are not suitable for this kind of flow because of rarefied effects.

1. Introduction

Gas flow around micro-scale structures forms an integral part of many applications of MEMS including micro-turbines, chemical sensors, micro-propulsion for spacecraft, flow control devices, and gaseous chromatographs. Experimental study of micro-scale gas flows is made inherently difficult by the small physical dimensions and has been mainly limited to flows in simple micro-channels and nozzles (Pong et al., 1994; Arkilic et al., 1997). While there has been a number of recent numerical studies of gas flows in micro-channels (Oh et al., 1995; Mavriplis et al, 1997; Cai et al., 2000), there has been almost no investigation of gas flows over external bodies at micro-scale. This forms the subject of the present numerical investigation.

Gas dynamics can be classified into continuum, slip, transition, and free-molecular flow regimes. The basic parameter defining these regimes is the ratio of the molecular mean free path (λ, at standard pressure and temperature, the mean free path of air is about 0.06 micron) to the smallest significant physical dimension characterizing the flow (L, can be around 1 micron or smaller for MEMS structures), namely the Knudsen number ($Kn=\lambda/L$). For such flows, the Knudsen number may be larger than 0.01, which places the flow in slip ($0.01\le Kn\le 0.1$) or transition ($0.1\le Kn\le 10$) regime. In these flows, the air in contact with the body surface may have a non-zero tangential velocity relative to the surface (slip), and collisions between molecules and collisions of the molecules with the wall have the same order of probability (transition). These rarefied phenomena must be included in any computer model designed to simulate these flow conditions.

Unfortunately, traditional computational fluid dynamics (CFD) techniques are only valid for the continuum regime (Kn<0.01), and acceptable for the slip regime if a slip wall condition is adopted instead of non-slip boundary condition. Then molecular-based numerical schemes, such as the direct simulation Monte Carlo (DSMC) method (Bird, 1994), are more physically appropriate for rarefied gas flows in micro-scale flows. However, the disadvantages of the DSMC method are obvious for micro-flows (Beskok, 2001). It is very difficult for DSMC to isolate the useful signal from the "noise" in low speed flows (micro-flows are usually low subsonic flows). The macroscopic flow velocity is sampled from the velocity of simulated microscopic particles ($V=V_i/N$) and the statistical scatter ($\sigma'=\sigma/\sqrt{N}$) is based on the sampling size. Here, V is the macroscopic flow velocity, V_i is the velocity of an individual particle, N is the sample size for the cell, σ is the physical statistical scatter ($\sigma=\sqrt{2RT}$, R is the specific gas constant, T is the temperature, and σ is about 400m/s for air at standard temperature) and σ' is the final numerical statistical scatter. If we suppose the sample processes in DSMC are totally independent from step to step, then a sample size of 1.6×10^5 is needed to control the statistical scatter within 1 m/s, and a sample size of 1.6×10^7 for the scatter to be within 0.1m/s! Hence, few micro-flows can be simulated due to the limit of CPU time (Oh et al., 1995).

An alternative approach is the information preservation (IP) method (Fan and Shen, 2001), which is very effective in reducing the statistical scatter in the DSMC method for low-speed, constant density flow systems. The IP method preserves macroscopic information as well as microscopic information in

* Graduate Student Research Assistant, Student Member AIAA
† Associate Professor, Senior Member AIAA
‡ Professor, Senior Member AIAA

simulated particles as the particles move and interact with each other and the domain boundaries. Recently, a 2D IP code was implemented and several cases were tested for low speed isothermal flows (Cai et al, 2000; Fan et al, 2001). We also implemented a 2D IP code that is suitable for flows over external bodies at the micro-scale. In the new code, the macroscopic information is updated according to the inviscid fluid mechanics equations using the Lagrangian description while collisions are considered between particles and with the body surface.

In this paper, the goal is to validate the IP code by simulating flows past a flat plate aligned with the free stream at low Reynolds numbers ($0.1 \le \mathrm{Re} \le 100$). We also investigate the aerodynamics of a 5% flat plate at low Reynolds number (Re = 4.0) as a function of angle of attack using the IP method and a continuum approach with slip boundary conditions.

2. Information preservation method

It is generally assumed that each particle simulated in the DSMC method represents an enormous number (10^8-10^{25}) of real molecules, and these particles possess random thermal properties according to certain distributions (they are Maxwellian distributions for equilibrium gas flows). Hence, each particle has the microscopic information (molecular position, velocity, internal energy, etc) and the collective information of the represented molecules (velocity, temperature, etc). The information preservation method aims to preserve and update the collective information of the real molecules, intending to reduce the statistical scatter inherent in particle methods. In the paper by Fan and Shen (1999), information velocity was preserved and updated by collisions between particles, collisions of particles with the wall and the external force field (the pressure field when gravity is neglected). Cai et al. (2000) additionally preserved the number density information and velocity information for computational cells when the IP method was extended to 2D isothermal problems. In our implementation (Boyd and Sun, 2001), number density information, velocity information and temperature information for both particles and computational cells are preserved. The information is updated by collisions between particles, collisions of particles with the wall, and the inviscid fluid mechanics equations in the Lagrangian description.

An implementation of the IP method can be summarized as follows (see also Figure 1):

(1) All the simulated particles and computational cells are assigned the necessary information after the computational domain is set up. For each particle, the molecular velocity, location (x, y) and internal energy are assigned as in the DSMC method. The number density information (n), velocity information (V_x, V_y) and temperature information ($T_i = \langle C_i^2 \rangle / R$, C is the thermal velocity, $i = x, y, z$) are assigned to both particles and computational cells as the initial flow condition.

(2) Move the particles using the molecular velocity with the same algorithms and models as the DSMC method.

(3) In a time step Δt, the preserved information may be changed due to the following causes:

(3a) If there are collisions between particles, a simple scheme satisfying general conservation laws is employed to distribute the post-collision information for two collided particles.

$$\frac{1}{n_1''} = \frac{1}{n_2''} = \left(\frac{1}{n_1'} + \frac{1}{n_2'}\right) \Big/ 2, \quad \text{(Specific volume } v = \frac{1}{\mathrm{m} \cdot \mathrm{n}}\text{)} \tag{1}$$

$$V_{x,1}'' = V_{x,2}'' = \left(V_{x,1}' + V_{x,2}'\right)/2, \quad \text{(Conserved momentum in x direction)} \tag{2}$$

$$V_{y,1}'' = V_{y,2}'' = \left(V_{y,1}' + V_{y,2}'\right)/2, \quad \text{(Conserved momentum in y direction)} \tag{3}$$

$$T_{x,1}'' = T_{y,1}'' = T_{z,1}'' = T_{x,2}'' = T_{y,2}'' = T_{z,2}'' \text{ (Conserved energy)} = \frac{T_{x,1}' + T_{y,1}' + T_{z,1}' + T_{x,2}' + T_{y,2}' + T_{z,2}'}{6} + \frac{1}{3R} \cdot \frac{\left(V_{x,2}' - V_{x,1}'\right)^2 + \left(V_{y,2}' - V_{y,1}'\right)^2}{2} \tag{4}$$

where superscripts ' and " denote pre- and post-collision, subscripts 1 and 2 denote particle 1 and particle 2, and subscripts x, y or z denote x, y or z direction, respectively.

(3b) If there are collisions of particles with a wall, the preserved information of collided particles are set in accordance with the collective behavior of a large number of real molecules. Namely, the information of the particles is set as the wall condition if it is a diffuse reflection while the information velocity component perpendicular to the wall is reversed if it is a specular reflection.

(3c) If particles reflect from a symmetric boundary, the information velocity component perpendicular to the symmetric boundary is reversed.

(3d) If there are new particles entering into the computational domain, their information is set as the boundary condition.

(3e) The preserved information of all particles are updated following the inviscid fluid mechanics equations in the Lagrangian description:

$$\frac{d[1/n]}{dt} = \frac{1}{n}\left[\frac{\partial V_x}{\partial x} + \frac{\partial V_y}{\partial y}\right] \tag{5}$$

$$\frac{dV_x}{dt} = -\frac{1}{n \cdot m}\frac{\partial p_x}{\partial x} \tag{6}$$

$$\frac{dV_y}{dt} = -\frac{1}{n \cdot m}\frac{\partial p_y}{\partial y} \tag{7}$$

$$\frac{d\left[\frac{1}{2}R \cdot T_x + \frac{u^2}{2}\right]}{dt} = -\frac{1}{n \cdot m}\frac{\partial [p_x \cdot u]}{\partial x} \tag{8}$$

$$\frac{d\left[\frac{1}{2}R \cdot T_y + \frac{v^2}{2}\right]}{dt} = -\frac{1}{n \cdot m}\frac{\partial [p_y \cdot v]}{\partial y} \tag{9}$$

$$p_i = n \cdot k \cdot T_i, \quad i = x, y \tag{10}$$

$$\frac{\partial}{\partial l} = \frac{\oiint_{cell} \frac{\partial}{\partial l} dxdy}{\oiint_{cell} 1 \cdot dxdy}, \quad l = x \text{ or } y \tag{11}$$

In the above equations, m is the mass of molecules, k is the Boltzmann constant, $\frac{d}{dt}$ is the full derivative and $\frac{\partial}{\partial t}$ is the partial derivative. However, it is difficult to calculate the derivatives of the information for discrete particles. The preserved information of the cell is then used when calculating the derivatives on the right hand side of Equations (5)-(9) using Equation (11). If the number density n on the right hand side of Equations (5)-(9) is replaced by the ratio of the number of represented molecules in the cell to the volume of the cell, the conservation properties can still be guaranteed. Notice that the concept of number density is not good for a single particle, so the number density information of a particle takes the value for the cell.

(4) The preserved information of computational cells is calculated from the particles.

$$\frac{1}{n_c} = \sum_{j=1}^{N_c} \left(\frac{1/n_j}{N_c} \right) \tag{12}$$

$$V_{i,c} = \sum_{j=1}^{N_c} \left(\frac{V_{i,j}}{N_c} \right), \quad i = x, y \tag{13}$$

$$T_{i,c} = \sum_{j=1}^{N_c} \left(\frac{T_{i,j}}{N_c} \right), \quad i = x, y, z \tag{14}$$

Here, subscript c denotes the cell information and N_c is the number of particles in the computational cell.

(5) Compute macroscopic quantities based on the preserved information. The macroscopic quantities are set to zero before sampling. For field data, those quantities are accumulated by adding the preserved information of the cell for every sampling step. Then the quantities divided by the number of sampling steps are the final sampled macroscopic quantities. For surface quantities, free molecular theory is employed based on the pre- and post-collision information of particles collided with the wall since there is no collision between particles happened during this process. Equations (15) and (16) describe the pressure information p and shear stress information τ for the collisions between particles and the wall. In these equations, subscripts i and r denote pre- and post-collision, u_3 is the information velocity component perpendicular to the surface of the incident particle, u_t is the information velocity component parallel to the surface, and $erf(\,)$ is the error function. Approximately, T can be regarded as the average of the component temperatures in three directions. Like field quantities, surface quantities are sampled by adding the information of collisions between particles and the wall for every incident particle. The final sampled surface quantities are obtained as the accumulated surface quantities divided by the total number of incident particles.

$$\begin{aligned} p_i &= n_i k T_i \left\{ \frac{s_3}{\sqrt{\pi}} e^{-s_3^2} + \left(\frac{1}{2} + s_3^2 \right) \left[1 + erf(s_3) \right] \right\} \\ p_r &= \frac{1}{2} n_i k T_i \sqrt{\frac{T_r}{T_i}} \left\{ e^{-s_3^2} + \sqrt{\pi} s_3 \left[1 + erf(s_3) \right] \right\} \\ p &= p_i + p_r, \qquad s_3 = u_3 \sqrt{\frac{m}{2kT_i}} \end{aligned} \tag{15}$$

$$\begin{aligned} \tau_i &= n_i k T_i s_{t,i} \left\{ \frac{e^{-s_3^2}}{\sqrt{\pi}} + s_3 \left[1 + erf(s_3) \right] \right\} \\ \tau_r &= n_i k T_i s_{t,r} \left\{ \frac{e^{-s_3^2}}{\sqrt{\pi}} + s_3 \left[1 + erf(s_3) \right] \right\} \\ \tau &= \tau_i - \tau_r, \qquad s_{t,i or r} = u_{t,i or r} \sqrt{\frac{m}{2kT_{i or r}}} \end{aligned} \tag{16}$$

(6) For steady flows, repeat steps 2-4 until the flow reaches a steady state. Then repeat steps 2-5 to sample and obtain the macroscopic quantities of the flow.

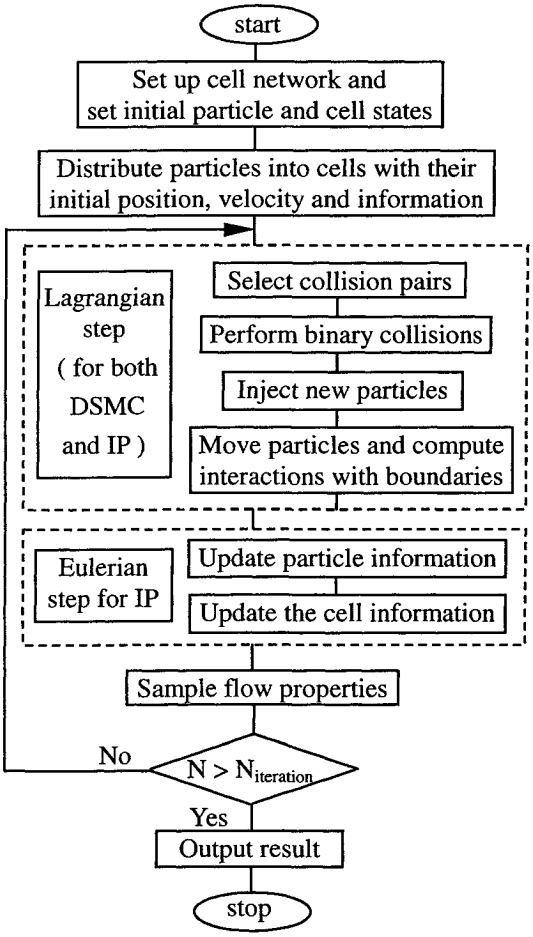

Figure 1. DSMC-IP flowchart

The above implementation of the IP method can greatly reduce the statistical scatter for low subsonic flows. In DSMC, the statistical scatter comes directly from the thermal movement of particles. In IP, the thermal movement of particles causes the statistical scatter only at the information level. Hence the statistical scatter of the information cannot be larger than the variation of the information in the whole flow field. Therefore, the IP method can greatly reduce the statistical scatter and hence the computational cost for low speed flows. The simulation of many practical micro-scale gas flows becomes possible. Another advantage of the IP method is that the preserved information of computational cells has small statistical scatter, and this can help apply effective boundary conditions for the DSMC method for low-speed flows. However, the IP method has disadvantages. One is that the IP method requires more memory (Cai et al., 2000). Another is that the current implementation of the IP method cannot recover the kinetic result for energy flux. Additional models may be required to address this issue. However, for low-speed flows over external bodies at micro-scale, the temperature variation is not large and this effect is negligible.

3. Numerical simulation of gas flows over flat plates

In this section, we aim to investigate the aerodynamics of a 5% flat plate airfoil at low Reynolds number flows with the IP method and a continuum approach with slip boundary conditions. Before the investigation, the skin friction of a flat plate with zero thickness at low Reynolds number flows is compared among the IP method and other techniques, in order to check the validity of the IP implementation for flows over external bodies at the micro-scale.

3.1 Flow over a flat plate with zero thickness

The problem of rarefied flow past a two-dimensional flat plate aligned with the free stream is one of fundamental interest since it generates a wide range of basic flow phenomena. As the Reynolds number decreases at a fixed Mach number, the nature of flow changes from continuum to free molecular. Schaaf and Sherman (1954) investigated flows over a flat plate experimentally and theoretically in the range of 34<Re<2020 for 2.5<M<3.8 and 3<Re<500 for M about 0.2 and 0.6. Other theories (Mirels, 1951; Dennis and Dunwoody, 1966; Tamada and Miura, 1978) are also available for flows from the slip regime to the free-molecular regime. However, theories for flows in the slip and transition regions can only predict flows qualitatively due to the approximations made. The IP method, on the other hand, can simulate the flows at different Reynolds number.

Consider airflow past a flat plat with a finite length of 20 microns. The free stream velocity is about 69m/s and the Mach number of the free stream is 0.2 with a temperature of 295K. The free stream density is determined from the Reynolds number based on the length of the plate. Figure 2 shows the computational domain used in the simulation. The whole domain is divided into 4800 non-uniform structured cells that are clustered to the plate. On average, 50 particles are located in each cell. When the Reynolds number is larger than 10, a subcell technique is employed with more simulated particles in each cell. For each case, the time step is smaller than the mean collision time of molecules. Finally, the given results are sampled after the skin friction reaches a constant value.

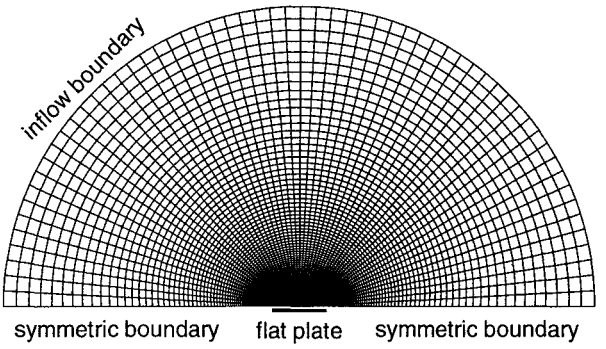

Figure 2. Computational grid
for flow over a flat plate without thickness

Figure 3 shows the drag coefficient of the plate for both sides at low Reynolds numbers from several techniques. The IP results approach the free molecular theory (Gombosi, 1994) ($C_D = 1.35/M$, M is the Mach number) when the Reynolds number becomes small (Re<0.2) and are close to the numerical solutions of the full Navier-Stokes equations of incompressible flows (Dennis and Dunwoody, 1966) when the Reynolds number is greater than 10. The following expression was derived by Tamada and Miura (1978) for the flat plate drag coefficient in slip flow on the basis of the Oseen-Stokes equations of motion:

$$C_D = \frac{8\pi}{R\{\ln(16/R) - \gamma + 1\}}\left\{1 - \frac{4k}{\pi}\frac{\ln(2/k) + \gamma + 1}{\ln(16/R) - \gamma + 1}\right\} \qquad (17)$$

where γ = 0.57722... is Euler's constant and k is the slip coefficient. If we take k in Equation (17) as the Knudsen number based on the length of the plate, the theory predicts similar results as the IP method for Reynolds number around 1 and 2. The experimental data from Schaaf and Sherman (1954) shown in Figure 3 were measured at a Mach number around 0.2 except that the case for the Reynolds number of 3.15 was measured with Mach number of 0.167. Good agreement is obtained between the experimental data and the IP results except for Reynolds number of 3.15. The difference here probably occurs since the Mach number of the flow is another important parameter for the drag on the plate at low Reynolds number. The incompressible experimental data of Janour (1951) is also plotted in Figure 3. It seems when the Reynolds number is larger than 10, the difference between the results from the compressible and incompressible flow is very small. Obviously, the Blasius solution of the boundary layer theory (Churchill, 1988) is not valid for low Reynolds number flows.

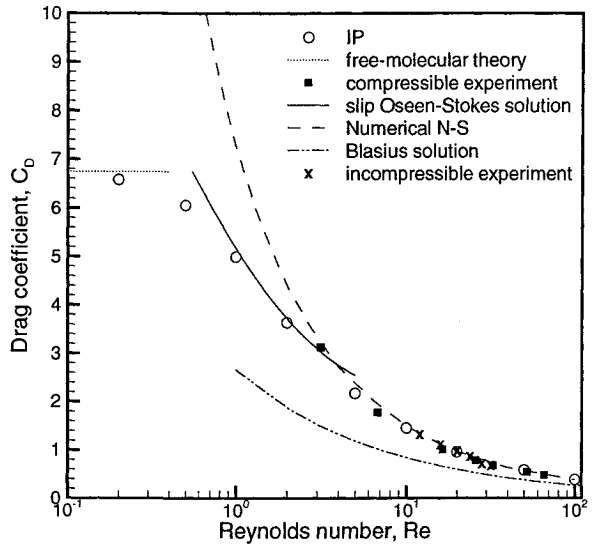

Figure 3 Drag coefficient of a finite plate at low Reynolds numbers

The local variation of skin friction over the plate is plotted in Figure 4. The skin friction increases and approaches the free molecular limit 3.375 ($C_f = 0.675/M$) as the Reynolds number decreases. This is quite different from the incompressible flow (Dennis and Dunwoody, 1966) where the combination of skin friction and the Reynolds number $C_f\sqrt{\mathrm{Re}_L}$ increases from the Blasius solution to infinity when the Reynolds number decreases. Generally, there is an obvious effect of the leading edge and trailing edge on the skin friction. Both ends of the finite plate have larger skin friction than the average, and this difference tends to vanish when the Reynolds number is smaller

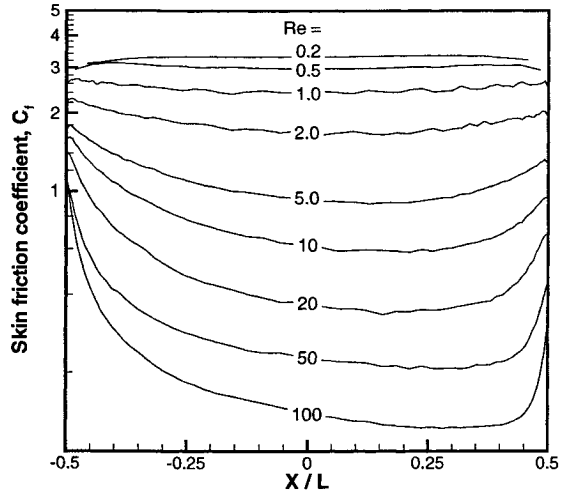

Figure 4 Skin friction of a finite plate at low Reynolds numbers

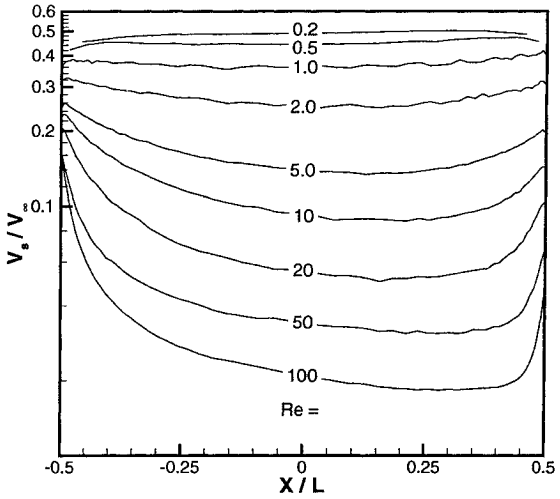

Figure 5 Slip velocity of a finite plate at low Reynolds numbers

than 1. The slip velocity V_s (Figure 5) on the plate shows similar behavior as the skin friction, which can be predicted by kinetic theory. If the plate is assumed as a fully momentum accommodated plate, the shear stress can be expressed as Equation (18) from the implementation of the IP method:

$$\tau = \frac{1}{2} m n_i V_s \langle c \rangle \left\{ \frac{e^{-s_3^2}}{\sqrt{\pi}} + s_3 [1 + erf(s_3)] \right\}, \quad \langle c \rangle = \sqrt{\frac{8kT_i}{\pi m}} \tag{18}$$

For low-speed flows (s is small, then s_3 is much smaller), the density variation and temperature variation are small, so the skin friction can be approximated as Equation (19). Hence the skin friction is proportional to the slip velocity.

$$C_f = \frac{\langle c \rangle}{V_\infty} \cdot \frac{V_s}{V_\infty} \tag{19}$$

3.2 Continuum approach with slip boundary conditions

Few experimental data or theoretical results are available for external flows at low Reynolds number (Re<100). We seek to use a continuum approach with slip boundary conditions to compare with the IP method for low Reynolds number flows.

The continuum approach solves the compressible Navier-Stokes equations using the preconditioning approach of Merkle et al. (1995). This approach is used because of the very large disparity between the velocity magnitude and the speed of sound in these flows. The preconditioning rescales the eigenvalues so that the convection speed is of the same order as the effective speed of sound. In addition, the Merkle approach improves the convergence of highly viscous flows. This results in a much better conditioned system that can be solved more easily. The steady-state solution does not depend on the preconditioning of the eigenvalues (Merkle, et al., 1995).

An O-grid of dimension 186×60 is used for the flow over a 5% flat plate. The grid is exponentially stretched to the airfoil surface and extended 10 chord lengths from the airfoil. We find that significantly better convergence is obtained by slightly rounding the corners of the rectangular cross-section airfoil. Thus, a radius of 0.1 micron is added at each corner to reduce the cost of the calculations. In comparison with solutions from an incompressible Navier-Stokes equations solver (McGrattan et al., 2000), this modification of the geometry is inconsequential.

The slip boundary conditions are implemented with the use of the Maxwell-type slip velocity expression (Schaaf and Chambre, 1958):

$$u_s = \frac{2-\sigma}{\sigma}\lambda\left.\frac{\partial u}{\partial n}\right|_w \qquad (20)$$

where the mean free path λ is given by $\lambda = \frac{2\mu}{\rho\langle c\rangle}$ with viscosity of the gas μ. We include a similar expression for the surface temperature slip, but at these low speed conditions, there is only a very small variation in temperature. Thus, the temperature slip is unimportant. The slip velocity in the direction tangent to the surface is computed with the above formula, and the normal direction velocity is set to zero. In keeping with the DSMC/IP calculations, the accommodation coefficient σ is set to 0.85.

3.3 Flow over a 5% flat plate

The measurements of Sunada et al. (1996) showed that a 5% flat plate has a much larger lift coefficient than NACA airfoils at Re=4,000 for incompressible flows. However, flows over micro-scale structures are usually at much lower Reynolds number. Hence it is of interest to investigate the aerodynamics of a 5% flat plate at lower Reynolds number since the airfoil performance depends on the Reynolds number.

The 5% flat plate is placed at certain angles of attack in an otherwise uniform stream of gas. The free stream condition is listed in Table 1, and the chord length of the plate is 20 microns. Figure 6 displays a part of the structured grid for the IP method from a computational domain that extends 5 chord lengths from the airfoil. For the IP method, a total of 11,200 cells is used and about 50 particles are located in each cell. The total sampling size is about 5,000,000 particles per cell after 300,000 iterations are executed with a time step of 2×10^{-11} s. Figure 7 shows the pressure history at several locations near the plate for the case with the angle of attack of 10°. With the given sampling size, the fluctuation of pressure is within 2 Pa, hence the numerical error of the pressure coefficient is smaller than 0.04 or 4%.

Table 1. Free stream conditions

Ma_∞	Re_∞	ρ_∞ (kg/m^3)	T_∞ (K)	U_∞ (m/s)
0.087	4.0	0.1176	295	30.0

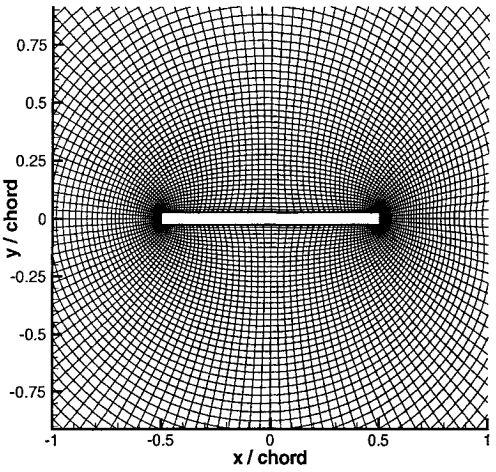

Figure 6 Part of computational grids for flow over a 5% flat plate

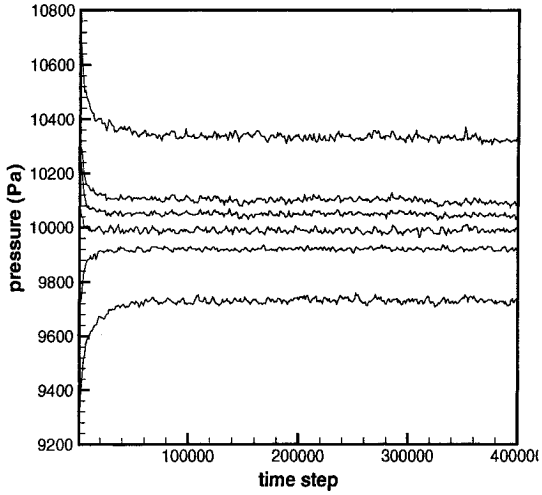

Figure 7 Pressure history at several locations near the plate

Consider the case for the angle of attack of 10°. The pressure contours are plotted in Figure (8) for both the IP method and the continuum approach. Figure (9) shows the velocity contours for both methods. Roughly speaking, the simulated flow fields from the two methods exhibit similar basic features. There is a high-pressure region around the leading edge and a low-pressure region around the trailing edge, which yields part of the drag on the plate. The pressure below the plate is higher than the pressure above the plate that generates the lift for the airfoil. The flow transfers part of its momentum to the plate, which decreases its velocity around the plate and increases the drag on the plate as another main factor. However, differences between the two solutions are also obvious. The variation of pressure from the IP method is smaller than that from the continuum approach. Namely, the pressure in the high-pressure region from the IP method is smaller than that from the continuum approach, and the pressure in the low-pressure

region from the IP method is higher than that from the continuum approach. Also, the continuum approach predicts smaller velocities around the airfoil than the IP method does. These differences are much clearer from the surface properties shown in Figures (10) and (11). There is some difference of the pressure coefficient on the airfoil between the two solutions, and the shear stress on the airfoil from the IP method is much larger than that from the continuum approach. However, there are no theoretical results for this airfoil at this Reynolds number, and the results here will be compared with an experiment that is being planned (Martin et al., 2001). In order to compare with the results in Figure 3 when the free stream Mach number is 0.087, we consider the flow over the 5% plate with no angle of attack. The average skin friction for the 5% flat plate is about 1.37 from the IP method, and it is about 1.52 for the plate with no thickness (this value is larger than 1.26 from Figure 3 when Re=4.0 because the Mach number is decreased). The average skin friction from the continuum approach, however, is too small at about 0.61. We also notice that the thickness of the plate will affect the skin friction on the surface. For free molecular flow, the ratio of the drag on the 5% flat plate (C_D=18.29) to the drag on the plate with no thickness (C_D=15.51) is about 1.18. When Reynolds number is 4,000, the ratio of the drag on the 5% flat plate (C_D=0.057, Sunada et al., 1996) to the drag on the plate with no thickness (C_D=0.0478, Dennis and Dunwoody, 1966) is about 1.19. Considering the measurement errors (±9%) in Sunada's experiment (1996), then the ratio ranges from 1.08 to 1.30. Finally, when the Reynolds number is 4.0, the ratio of the drag on the 5% plate (C_D=3.38, IP) to the drag on the plate with no thickness (C_D=3.04, IP) is about 1.11. This is a reasonable value compared with the free molecular theory and the experimental data. Again, the ratio from the continuum approach is unusual since the value is less than 1. It may be that the slip boundary conditions are not enough for these flows. Perhaps additional terms must be incorporated into the Navier-Stokes equations, such as in the Burnett equations. Another possible reason is that the continuum approach is not valid for a very small region, but this affects the whole flow since the equations are elliptic.

The aerodynamic characteristics of the 5% flat plate are plotted in Figure (13) when the Reynolds number is 4.0. For comparison, the aerodynamics of the plate are plotted in Figure (12) for free molecular flows and in Figure (14) when the Reynolds number is 4,000 (Sunada et al., 1996). Clearly, the aerodynamics at Re=4.0 is closer to that of free molecular flow than that when Re=4,000, although the values are much smaller. The ratio of lift to drag is less than 1 when Re=4.0, which agrees with Miyagi's result (1964). From the IP results, the lift slope is about 3.82, which is smaller than 5.8 when Re=4,000. The same trend exists for NACA0009 airfoil at higher Reynolds numbers (Sunada et al., 1996) with 2.9 at Re=4,000 and 5.5 at 40,000.

4. CONCLUSIONS

The information preservation method is a good tool to investigate gas flows over micro-scale airfoils that range from near-continuum flow to transition flow. Good agreement is obtained among the IP method and other techniques for the drag on a flat plate with no thickness in low Reynolds number flows.

The aerodynamics of a 5% flat plate at Re=4.0 is quite different from that at Re=4,000. The lift slope of the plate at Reynolds number of 4.0 is about 3.82, and the ratio of lift to drag is less than 1. This may be one reason that small insects flap their wings in order to increase the lift. In addition, the continuum approach with slip boundary conditions predicts similar basic flow patterns as the IP method, but there are differences in details. This may indicate that continuum approaches are not suitable for this kind of flow because of rarefied effects. Additional terms may need to be incorporated into the Navier-Stokes equations to address this problem.

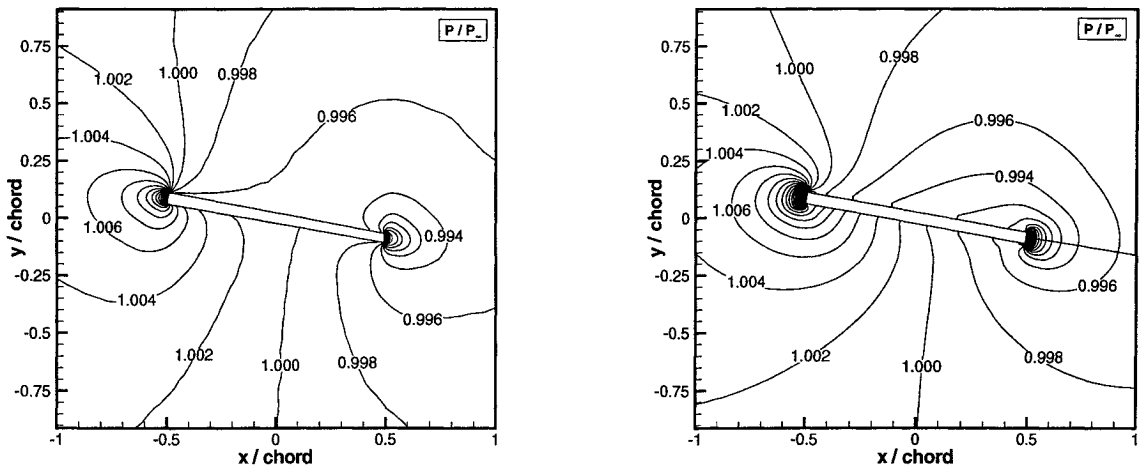

Figure 8 Pressure field (left: IP; right: continuum)

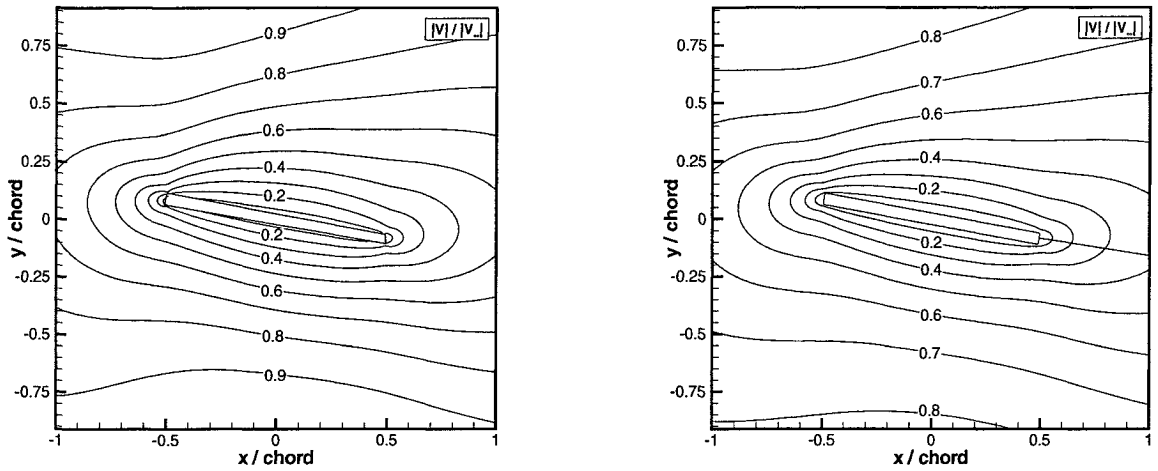

Figure 9 Velocity field (left: IP; right: continuum)

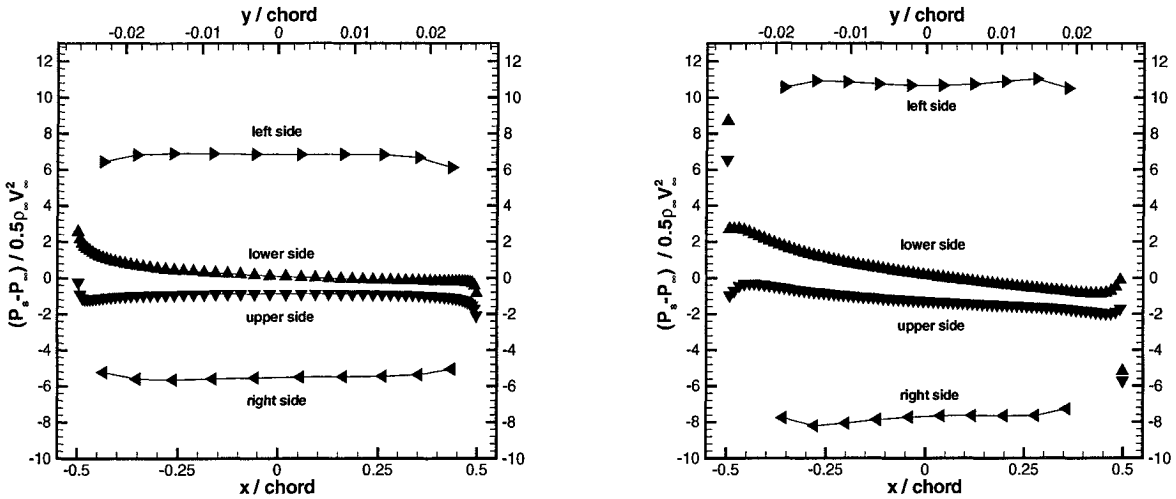

Figure 10 Pressure distributions along the plate surface (left: IP; right: continuum)

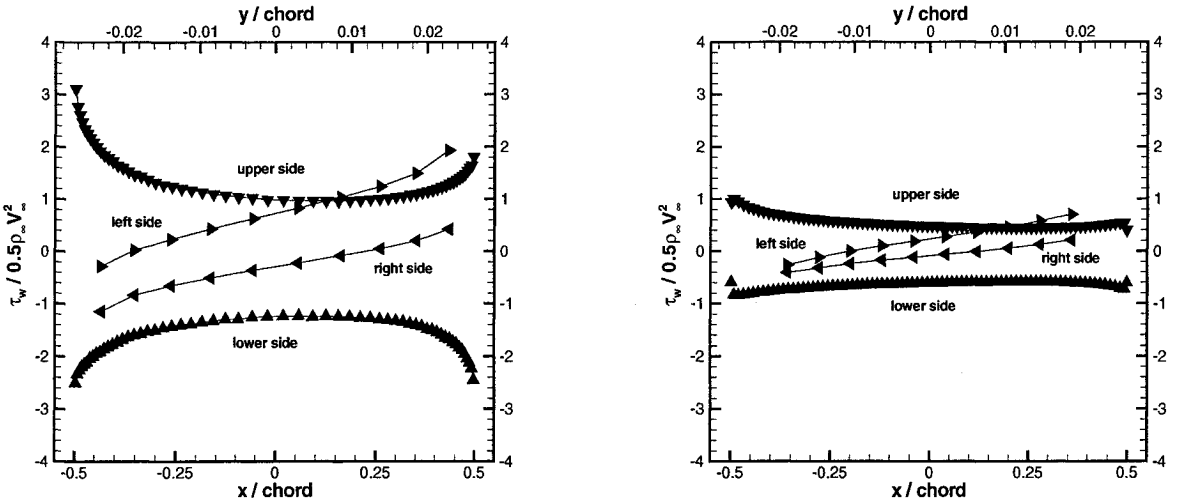

Figure 11 Skin friction distributions along the plate surface (left: IP; right: continuum)

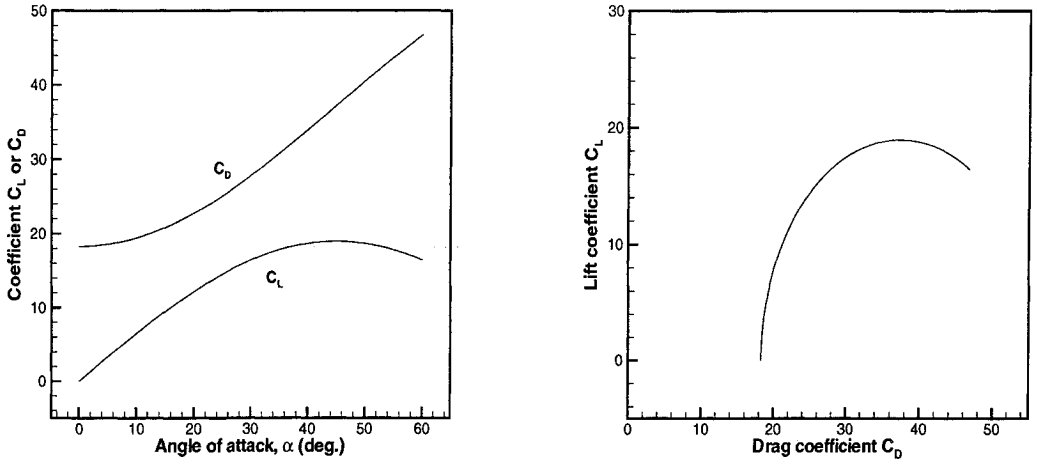

Figure 12 Characteristics of 5% flat plate at Re~0 from free-molecular theory (left: α-C_L, right: C_D-C_L)

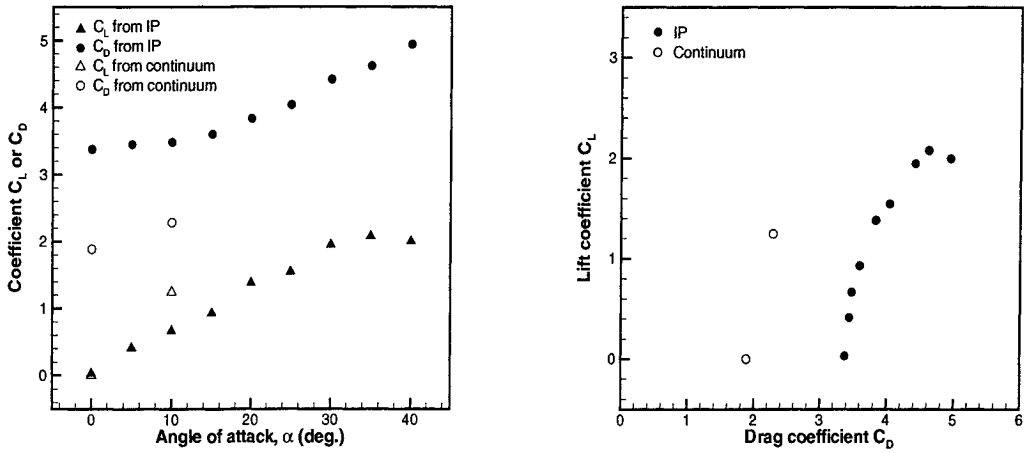

Figure 13 Characteristics of 5% flat plate at Re=4.0 from the IP method (left: α-C_L, right: C_D-C_L)

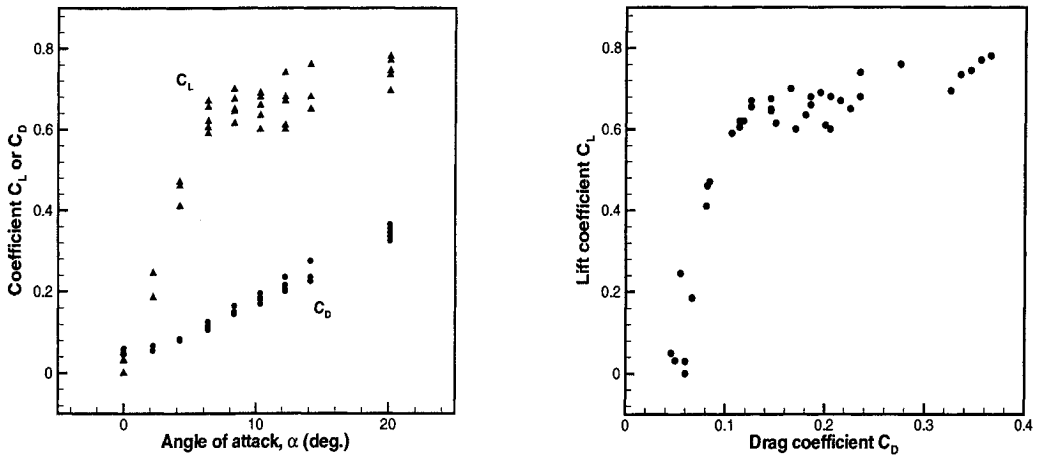

Figure 14 Characteristics of 5% flat plate at Re=4,000 from the experiment (left: α-C_L, right: C_D-C_L)

ACKNOWLEDGMENTS

This work was supported by the Air Force Office of Scientific Research through MURI grant F49620-98-1-0433.

References:

Arkilic, E., Schmidt, M.A., and Breuer, K.S., 1997, "Gaseous Flow in Long Microchannels," *Journal of Micro Electro Mechanical Systems*, vol. 6, pp. 2-7

Beskok, A., 2001, "Physical Challenges and Simulation of Micro Fluidic Transport," AIAA Paper 2001-0718, Reno, Nevada, January 2001

Bird, G.A., 1994, "Molecular Gas Dynamics and the Direct Simulation of Gas Flows," Oxford Science Publications, New York

Boyd, I.D. and Sun, Q., 2001, "Particle Simulation of Micro-Scale Gas Flows," AIAA Paper 2001-0876, Reno, Nevada, January 2001

Cai, C., Boyd, I.D., Fan, J. and Candler, G.V., 2000, "Direct Simulation Method for Low-speed Microchannel Flows," AIAA *Journal of Thermophysics and Heat Transfer*, vol. 14 (3), pp. 368-378

Churchill, S.W., 1988, "Viscous Flows: The Practical Use of the Theory," Butterworth Publishers, Stoneham

Dennis, S.C. and Dunwoody, J., 1966, "The Steady Flow of a Viscous Fluid past a Flat Plate," *Journal of Fluid Mechanics*, vol. 24 (3), pp. 577-595

Dietrich, S., and Boyd, I.D., 1996, "Scalar and Parallel Optimized Implementation of the Direct Simulation Monte Carlo Method", *Journal of Computational Physics*, vol. 126, pp. 328-342

Fan, J., and Shen, C., 1999, "Statistical Simulation of Low-Speed Unidirectional Flows in Transition Regime," in *Rarefied Gas Dynamics*, edited by R. Brum, et al., (Cepadus-Editions, Toulouse, 1999), vol. 2, pp. 245-252

Fan, J., and Shen, C., 2001, "Statistical Simulation of Low-Speed Rarefied Gas Flows," *Journal of Computational Physics*, vol. 167, pp. 393-412

Fan, J., Boyd, I.D., Cai, C.P., Hennighausen, K. and Candler, G.V., 2001, "Computation of Rarefied Gas Flows Around a NACA 0012 Airfoil," *AIAA Journal*, vol. 39 (4), pp. 618-625

Gombosi, T.I., 1994, "Gaskinetics Theory," Cambridge University Press, Cambridge

Ho, C.M., and Tai, Y.C., 1998, "Micro-Electro-Mechanical-Systems (MEMS) and Fluid Flows," *Annual Review of Fluid Mechanics*, vol. 30, pp. 579-612

Janour, Z., 1951, "Resistance of a Plate in Parallel Flow at Low Reynolds Numbers," *NACA* TM 1316

Liu, V.C., 1959, "On the Drag of a Flat Plate at Zero Incidence in Almost-free-molecule Flow," *Journal of Fluid Mechanics*, vol. 5 (3), pp. 481-496

Martin, M.J., Kurabayashi, K. and Boyd, I.D., 2001, "Measurement of Lift and Drag on MEMS Scale Airfoils in Slip Flow," *Proceedings of 2001 ASME Fluids Engineering Division Summer Meeting*, New Orleans, Louisiana, May 2001

Mavriplis, C., Ahn, J.C., and Goulard, R., 1997, "Heat Transfer and Flowfields in Short Microchannels Using Direct Simulation Monte Carlo," *Journal of Thermophysics and Heat Transfer*, vol. 11 (4), pp. 489-496

McGrattan, K.B., Baum, H.R., Rehm, R.G., Hamins, A. and Forney, G.P., 2000, "Fire Dynamics Simulator—Technical Reference Guide," NISTIR 6467

Merkle, C.L., Venkateswaran, S. and Buelow, P.E.O., 1995, "Reliability Enhancement of Navier-Stokes Algorithms Through Convergence Acceleration," NACA CR-196635

Mirels, H., 1951, "Estimate of Slip Effect on Compressible Laminar-Boundary-Layer Skin Friction," NACA TN 2609

Miyagi, T., 1964, "Oseen Flow Past a Flat Plate Inclined to the Uniform Stream," *Journal of the Physical Society of Japan*, vol. 19(6), pp 1063-1073

Oh, C.K., Oran E.S., and Cybyk, B.Z., 1995, "Microchannel Flow Computed with the DSMC-MLG," AIAA paper 95-2090, San Diego, California, June 1995

Pong, K.C., Ho, C.M., Liu, J., and Tai, Y.C., 1994, "Non-linear Pressure Distribution in Uniform Microchannels," in ASME FED, vol. 197, *Application of Microfabrication to Fluid Mechanics*, pp. 51-56

Schaaf, S.A. and Chambre, P.L., 1958, "Flow of Rarefied Gases," *High Speed Aerodynamics and Jet Propulsion*, vol. 3(H), Princeton University Press, pp. 678-739

Schaaf, S.A. and Sherman, F.S., 1954, "Skin Friction in Slip Flow," *Journal of the Aeronautical Sciences*, vol. 21 (2), pp. 85-90

Sunada, S. Sakaguchi, A. and Jawachi, K., 1997, "Airfoil Section Characteristics at a Low Reynolds Number," *Journal of Fluids Engineering*, vol. 119, pp. 129-135

Tamada, K. and Miura, H., 1978, "Slip Flow Past a Tangential Flat Plate at Low Reynolds Numbers," *Journal of Fluid Mechanics*, vol. 85 (4), pp. 731-742